Wavefront sensor with Fresnel zone plates for use in an undergraduate laboratory

Piotr Migdał, Piotr Fita,[a] and Czesław Radzewicz
Faculty of Physics, Warsaw University, ul. Hoza 69, 00-681 Warsaw, Poland

Łukasz Mazurek
XIV Stanisław Staszic High School, ul. Nowowiejska 37a, 02-010 Warsaw, Poland

(Received 6 February 2007; accepted 9 November 2007)

We propose a modification of the Shack–Hartmann wavefront sensor in which the lens array is made of Fresnel zone plates. The modification allows students to construct the sensor in an undergraduate laboratory at little cost. In spite of its simplicity the sensor has a sensitivity of $\lambda/50$ in relative measurements, which is sufficient to measure a wavefront of a laser beam distorted by various optical elements as well as by a turbulent airflow. Such an experiment is an excellent supplement to a course in optics, gives students a deeper understanding of the wavefront concept, and demonstrates the wavefront measurement technique widely used in physics, astronomy, and medicine. © *2008 American Association of Physics Teachers.*

[DOI: 10.1119/1.2820390]

I. INTRODUCTION

The concept of a wavefront is important in optics and in the physics of waves in general. Phenomena such as focusing or defocusing of a collimated beam by a lens and the free propagation of a Gaussian beam can be well described as changes of the curvature of a wavefront. The wavefront approach is also the most natural way of describing the operation of optical elements made of a material with a spatially varying index of refraction (for example, GRIN lenses which are often used to couple light to optical fibers).[1] Wavefront analysis is the enabling technology in the rapidly developing field of adaptive optics and is used in modern astronomical telescopes[2] and high power laser systems.[3,4] Wavefront measurements are also crucial for eye surgery because they are an excellent tool for diagnosing eye aberrations prior to and during surgical corrections.[5]

Because of its prominence in wave physics and important applications in science and technology, the concept of a wavefront should be carefully taught during a course on the physics of waves and optics. In this paper we show that the introduction of this concept during a course in optics can be easily and effectively supplemented by wavefront measurements in an undergraduate student laboratory.

The foundation for the easiest and most direct way of determining wavefront distortion was given by Johannes Hartmann at the beginning of the 20th century when he used an array of small circular holes in an opaque screen placed over the aperture of a large astronomical refractor to test the quality of its optics.[6] Light rays passing through different holes created separate spots on a photographic plate located out of the focal plane. Light rays entering the input aperture of the telescope at different positions could be traced in the vicinity of the focal plane after exposing two plates—one on either side of the focus.

The Hartmann detector in its original shape of a mask (an opaque screen with regularly distributed holes) can be easily adapted to measure the shape of a wavefront of a laser beam. The method uses a purely geometrical effect—a nonplanar wavefront is tilted differently over different holes. Thus a spot created on the screen by the light entering a particular hole is shifted proportionally to the gradient of the wavefront over this hole (see Fig. 1). After recording these displacements the gradient and subsequently the shape of the whole wavefront can be recovered.

The Hartmann wavefront sensor suffers from two problems. Only a small fraction of the incident light passes through the holes in the mask and creates the spots on the screen, which limits the applications of the sensor to strong beams and/or requires sensitive detectors. Also the spots are washed out due to diffraction, making the precise determination of their positions difficult or even impossible if spots created by different holes overlap (see Fig. 1).

Both problems were solved by a modification of the Hartmann sensor due to Shack and Platt.[7,8] In the Shack–Hartmann (or Hartmann–Shack) sensor the holes are replaced by small lenses—lenslets. The light entering the entire aperture of a lenslet focuses on a corresponding focal spot. Thus the diameter of the lenslets may be equal to the separation between them without losing spatial resolution. Hence almost all the incident light is used to create spots on the screen, and the spots are also significantly smaller than those in the Hartmann sensor. Therefore much weaker beams can be measured with greater sensitivity to wavefront distortions. However, the Shack–Hartman sensor has one serious disadvantage: it requires a regular array of lenslets with diameters of the order of 1 mm. Despite great developments in optical technology, lenslet arrays are expensive. Commercial models contain either refractive plano-convex lenses or diffractive Fresnel lenses produced by photolithography and etching. Making a suitable array of lenses is practically impossible without highly specialized equipment. Although its cost is acceptable in scientific, medical, or industrial applications, it might be a serious obstacle for a student laboratory.

In this paper we propose an alternative approach—a sensor in which the lenses are replaced by flat transmissive Fresnel zone plates. Such a sensor can be easily prepared by students at little cost. It produces images with spots that are brighter and sharper than those obtainable with a Hartmann screen, and an inexpensive video or digital camera can be used as a detector. It is also much easier to precisely measure

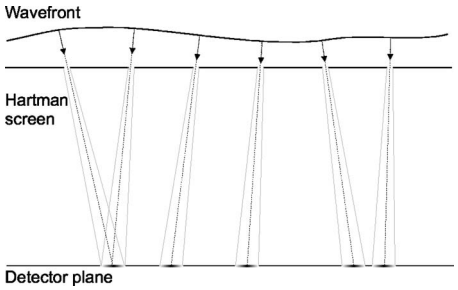

Fig. 1. Principle of a Hartmann wavefront detector.

the displacements of the spots, and the range of measurable wavefront distortions is larger due to the reduced risk of spot overlap.

II. FRESNEL ZONE PLATE

A Fresnel zone plate is a well known optical element,[9–13] so it is discussed here only to the extent required for using it in a wavefront sensor. It consists of a set of concentric rings (zones), alternatively transparent and opaque. The radii of the zones are such that each zone is half of the wavelength longer than the previous one from the primary focus point located on the axis. This condition can be easily converted to an expression for the radii R_n of the nth border between zones:

$$R_n = \sqrt{nf\lambda + n^2\frac{\lambda^2}{4}}, \tag{1}$$

where f is the focal length and λ is the wavelength of light. In practical systems (visible light, f of the order of millimeters) Eq. (1) simplifies to

$$R_n = \sqrt{nf\lambda} = \sqrt{n}R_1, \tag{2}$$

which is accurate to within 10^{-3}.

A Fresnel zone plate behaves much like a standard lens of a focal length f. In particular, it focuses an incident collimated beam. If the beam is not parallel to the optical axis, the focal spot lies on the line parallel to the beam coinciding with the center of the zone plate,[10] which is essential for the operation of the wavefront sensor. Moreover, the resolving power of a zone plate is similar to that of a lens with the same aperture.[9] Namely, the radius r_{spot} of a spot created by focusing a collimated beam (defined as the distance of the first intensity minimum from the center of the spot) may be approximated by the well known expression:

$$r_{\text{spot}} = \frac{1.22\lambda f}{2R_{2m-1}}, \tag{3}$$

where R_{2m-1} is the radius of the zone plate with m transparent zones.

Equation (3) is accurate only for a large number of zones constituting a plate; it is just a rough approximation for plates with few zones. We analyzed the latter by numerical evaluation of Fresnel diffraction patterns[14] created by zone plates of the same focal length and various number of transparent zones m. The size of the image created in the focal plane scales linearly with the size of the first (central) zone R_1, and thus we use R_1 as the unit of distance.

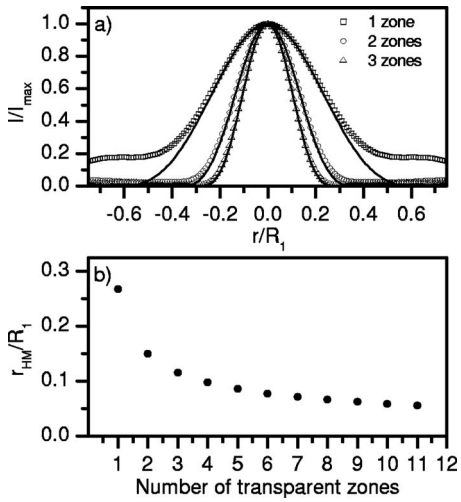

Fig. 2. (a) Normalized radial distribution of the light intensity within the spots created by Fresnel zone plates with a given number of transparent zones (symbols) and by refractive lenses of the same aperture and focal length (solid lines). (b) The radius at half of the maximum intensity of the spot created by a zone plate as a function of the number of zones.

The radial distribution of the light intensity in the focal plane of a zone plate is shown in Fig. 2(a); the corresponding plots for refractive lenses of the same diameter and focal length are depicted by solid lines. A significant difference between the two is observed only for a plate with one zone ($m=1$), that is, for a circular aperture. Even in this case the light distribution is confined to its central part, which means that the classical Hartmann sensor also takes advantage of the reduction of the diameter of the spots, provided that the distance of the image plane from the mask is equal to $f = R_1^2/\lambda$.

Zone plates with $m \geq 2$ are inferior to refractive lenses of the same aperture solely due to the behavior of the tails of the intensity distribution (and lower transmission, which is not important for wavefront sensing in a student laboratory). Therefore their focusing properties are not affected, but when a few tens of plates create a dense array, the light contained in the tails adds up to make a considerable background. This background must be taken into account when analyzing data (see Sec. V). Nevertheless, it is not too high a price to be paid for the simplicity of making a dense array of lenslets.

To describe quantitatively the dependence of the size of the spot on the number of zones in the plate we characterize the former by its radius at one half of the maximum intensity r_{HM}, not by the first minimum position because the latter is poorly defined for a small number of zones. The value of r_{HM} calculated for plates with the number of transparent zones m ranging from 1 to 11 is shown in Fig. 2(b). A rapid change is observed for $m \leq 3$. Therefore there is no need to make wavefront sensors consisting of zone plates with more than $m=3$ transparent zones, and those with $m=2$ still work well, as we have verified experimentally. We suggest choosing $m=3$ or if a very dense array is needed, $m=2$.

III. PREPARATION OF A WAVEFRONT SENSOR

We have tested two methods of preparing a wavefront sensor made of Fresnel zone plates. In one approach an enlarged mask drawn on a computer and printed on a sheet of paper

was photographed with a 35 mm camera on black and white photographic film. The film was then developed and cut into frames which were used as sensors after placing them in standard slide frames. The main advantage of this method is that the entire process, starting with the calculations of the Fresnel plate geometry in Eq. (2), can be done in a laboratory, thus allowing students to design and make the masks. However, a darkroom in which the film can be developed is requisite. In a typical case a mask printed on a sheet of paper is reduced on the film to the size of a few millimeters. This reduction must be taken into account while drawing the zone plates. If a low-grain low-speed film is used (in our case Ilford PANF Plus, ISO 50), the resolution of the resulting image is limited by the resolving power of the camera lens. For a lens with an average resolving power of 50 lines/mm the finest details are of the order of 20 μm which is sufficient to produce a few well resolved Fresnel zones. Care should be taken to keep the contrast of the negative as high as possible. To this end the enlarged mask must be printed on a laser printer with the highest possible quality and be strongly and uniformly illuminated when photographed. A high-contrast developer should also be used. Still, our results show that the contrast of masks obtained with the photographic method is not very high and the resultant wavefront sensor produces a significant background which makes it more difficult to determine the positions of the focal spots. This difficulty does not prevent the use of the photographic technique, but a higher quality sensor can be made with the other method. In this method the mask is drawn on a computer with a 1:1 scale, and the drawing is then printed on a transparent plastic film in a shop that makes printing plates. For the standard resolution of 3600 dots per inch details as small as a few micrometers can be easily printed. Moreover, the contrast is usually much higher than that obtained with a photographic method. The cost of making a letter size plastic sheet on which a few hundreds of masks can be fitted is only a few dollars, and thus the cost of a single mask is negligible.

The parameters of the mask, that is, the total number of zone plates and their focal length, can be chosen from a wide range depending on the characteristics of the wavefronts to be measured and the type of the camera. The relative displacement of a spot on the detector is proportional to the focal length of lenslets; the smaller the spot, the more accurately its position can be measured. Thus we can assume that the minimal measurable tilt of the wavefront $\delta\theta$ is proportional to the focal length f and inversely proportional to the radius of the spot r_{spot}. The latter is related to the parameters of the zone plates by Eq. (3). Therefore we conclude that the sensitivity of the sensor is directly proportional to the radius of the zone plates R_{2m-1}:

$$\delta\theta \sim \frac{f}{r_{\mathrm{spot}}} \sim \frac{R_{2m-1}}{\lambda}. \tag{4}$$

The size of the mask should match the size of the detector, so the larger each zone plate, the fewer zone plates fit within the mask because they should not overlap too much. This requirement gives an inverse relation between the number of points at which the wavefront is sampled and the sensitivity of the sensor for fixed number of transparent zones.

In our experiment we used two different CCD cameras: a standard analog CCTV camera with a 1/4 in. chip as well as a digital USB camera (Sumix SMX-150) with a 2/3 in. chip (image array size 8.6 mm$\times$6.9 mm, pixel size 6.7 μm $\times$6.7 μm). With the first camera we used masks with focal lengths in the range of 20–50 mm, and with the second one the focal lengths were in the range of 50–300 mm. The diameter of a single Fresnel lens (calculated for the wavelength 633 nm of the He–Ne laser) was in the range of 0.5–0.8 mm and 0.8–2 mm, respectively.

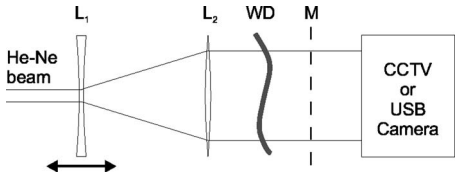

Fig. 3. Experimental setup for wavefront measurements. Lenses L_1 and L_2, wavefront-distorting element WD, and mask M.

IV. WAVEFRONT MEASUREMENTS

The setup for wavefront measurements is shown in Fig. 3. The beam of a 1 mW He–Ne laser (a visible diode laser might be a better light source) is expanded by a telescope consisting of two lenses L_1 (f_1=−27 mm) and L_2 (f_2 =364 mm), or alternatively by a commercial beam expander. The divergence of the beam is controlled by translating L_2 along the beam, or by adjusting the telescope. The radius of the beam at the sensor's position can be changed by selecting different lenses in the expanding telescope. To obtain a nonspherical wavefront a wavefront-distorting element WD could be additionally inserted into the beam. For the latter we used a cylindrical lens or a microscopic glass melted with a gas torch. We can also put a soldering gun beneath the beam for a real-time demonstration of wavefront distortions caused by a turbulent airflow. After a slight modification of the setup the beam may be reflected from a spherical mirror. This configuration allows us to observe the astigmatism introduced into the beam when the angle of incidence is nonzero. (The astigmatism can be also observed in a straight geometry with a long focal length lens that is tilted with respect to the beam axis.)

The mask must be located parallel to the detector plane at the distance equal to the focal length of the zone plates. The latter is not crucial because the focusing is weak. The position of the mask can be easily optimized by observing the image created by the mask. The required accuracy is of the order of a few percent of the focal length. For practical reasons all the components are placed on an optical table, but they may also be mounted on an optical bench.

The signal from the CCTV camera was recorded using a frame grabber; the Sumix camera is simply connected to an USB port of a computer. The software provided with those devices is used to save images from the cameras. Sample images of a nearly planar wavefront and the masks used to obtain them are shown in Fig. 4.

V. WAVEFRONT RECONSTRUCTION

There are two major steps leading from the measured data to the reconstructed wavefront: determination of the positions of the focal spots and calculation of the wavefront shape.

The price to be paid for the simplicity of the wavefront sensor consisting of zone plates is the diffractive background which adds to the image of the foci (it is clearly visible in

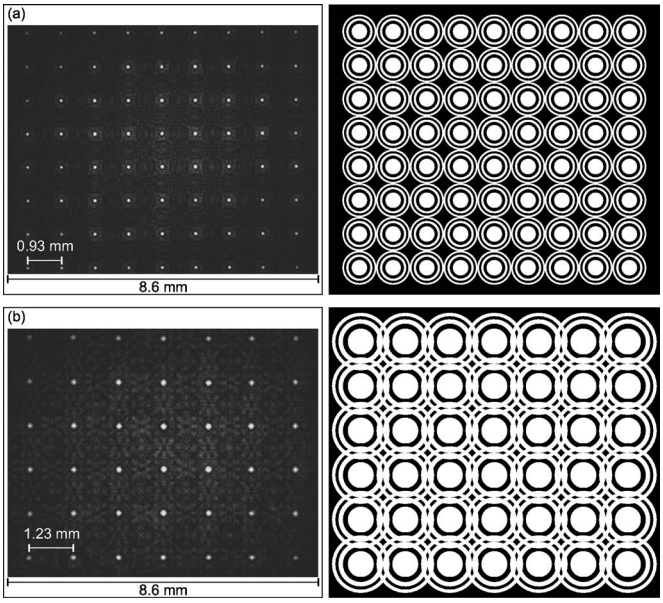

Fig. 4. Sample images from the wavefront sensor obtained with the masks shown. The scale is maintained between the images and the masks. (a) $f=70$ mm and (b) $f=200$ mm.

Fig. 4). To reduce its influence we subtract a threshold value from the intensities of all pixels in the image. Then the values of the pixels which are negative after the subtraction are set to zero. The optimum value of the threshold is usually in the range of 0.35–0.5 of the maximum intensity of the spots. The picture after this pre-processing is divided into a lattice of square subimages so that each spot fits entirely into the corresponding subimage. The absolute position of the spot is obtained by calculating the center of mass of the subimage (the weighted mean of the position with pixel intensities as weights).[15]

The detector can be used in two regimes each requiring different data and analysis. If the geometries of the sensor and detector are known with high accuracy, a single measurement is sufficient—the displacements of the focal spots with respect to the positions of the corresponding lenses provide information on the absolute shape of the wavefront. In contrast, we can also use the sensor to determine the distortions introduced by a given optical component placed into a beam with a wavefront of any reasonable shape. In this case two measurements are required: one on a beam with the component under investigation and the other without it. In this mode of operation the relative displacements are used in the data analysis, and the result shows only the contribution to the shape of the wavefront resulting from the presence of the component—wavefront distortion due to the component.

In the latter regime high accuracy can be achieved without paying much attention to the adjustment of the setup, while the sensitivity of the absolute measurements is significantly limited by the distortions of the wavefront introduced by the plastic mask as well as by misalignment of the setup. Thus the relative measurements are more attractive for a student laboratory, especially in measurements of small distortions of the wavefront caused, for example, by air fluctuations. The absolute measurements can be easily performed on beams passing through spherical or cylindrical lenses with focal lengths of the order of meters, because in this case the curvature of the wavefront is significantly larger than the errors due to an imperfect calibration and/or misalignment of the setup.

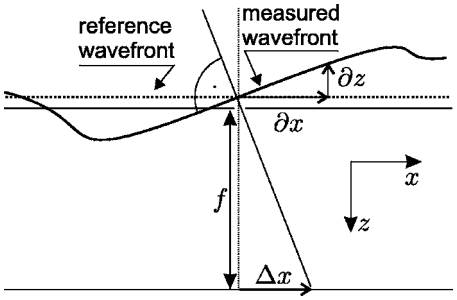

Fig. 5. Geometry used in the reconstruction of the wavefront.

The displacements of the spots (absolute or relative) in the x and y directions, Δx and Δy, are used to find the components of the gradient of the wavefront surface [described by the function $z(x,y)$] in the positions of the corresponding lenses (see Fig. 5):

$$\frac{\partial z}{\partial x} = -\frac{\Delta x}{f}, \tag{5a}$$

$$\frac{\partial z}{\partial y} = -\frac{\Delta y}{f}, \tag{5b}$$

where the focal length f is equal to the distance between the mask and the detector plane.

The most intuitive way to calculate the shape of the wavefront would be a direct integration of its gradient. Because of the experimental noise in the gradient, the integration is ambiguous—the integration from point A to B along different paths usually gives slightly different results. Therefore we use the following approach: the experimental values of the gradient are treated as a vector field, which can be decomposed into purely rotational and purely irrotational parts. Because the curl of a gradient is always zero, the rotational part originates purely from the noise. Thus it is rejected and only the irrotational part is integrated to calculate the shape of the wavefront.[16] Other algorithms, less intuitive but simpler to implement, utilize matrix calculus.[17,18] A very well described and ready to use algorithm presented in Ref. 17 is the most suitable for the student laboratory.

The wavefront is reconstructed with an accuracy limited by experimental errors. For relative measurements these errors originate mostly from mechanical instabilities of the setup and air currents flowing through the beam path. We estimated the extent to which those factors influence the results by recording a sequence of 20 images of a flat wavefront with 5 s intervals. Then we retrieved the average positions of the focal spots and their standard deviations, which were used to calculate the standard deviations of the wavefront in the z direction. The result is 0.004–0.015 μm depending on the mask parameters. A typical deviation of a single measurement result from the mean wavefront for two different masks is shown in Fig. 6. As expected, the noise is significantly higher for the mask with the higher spatial resolution and thus the shorter focal length.

The value of the standard deviation depends on the length of the image sequence and is greater for longer sequences. We believe that this correlation exists because the recon-

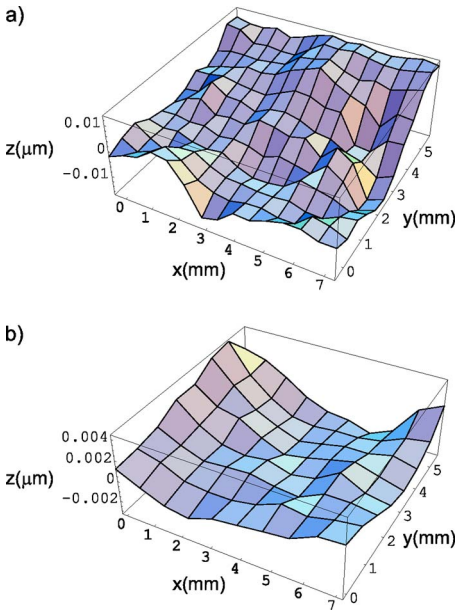

Fig. 6. Typical deviations of a single measurement of a flat wavefront from the arithmetic mean of 20 measurements in 5 s intervals for the mask with focal lengths of (a) 10 cm and (b) 13 cm.

structed wavefront was slowly varying with a characteristic time scale of the order of several seconds, indicating mechanical instabilities in the setup and possibly the relaxation of the flexible mask. Nevertheless, the model setup is capable of detecting relative changes of the wavefront shape of the order of $\lambda/50$. Such a sensitivity allows us to use it for many experiments in a student laboratory; a few examples are described in Sec. VI.

The accuracy of the absolute measurements was checked by reconstructing the wavefront from the image of spots created by a collimated laser beam. The resulting wavefront showed distortions of 0.1–0.5 μm which allowed us to estimate the experimental error in this regime to be slightly smaller than λ.

VI. APPLICATIONS OF THE WAVEFRONT SENSOR

From the many possible applications of the sensor such as measurements of the curvature of the wavefront of the beam passing through a spherical or a cylindrical lens or detection of the distortions introduced by a poor quality glass plate, we discuss two that are especially interesting and instructive.

The first experiment visualizes the distortions of the wavefront due to fluctuations of the temperature and density of the air in which the beam propagates. The fluctuations are caused by a soldering iron located a few millimeters below the beam. The distortions can be observed in real time if a fast enough acquisition system and reconstruction software is used or a sequence of the images is recorded for later processing. Such a procedure is an analogue of the wavefront measurements in adaptive optics systems of large astronomical telescopes. The experiment also indicates the necessity of suppressing ambient air currents if high measurement accuracy is to be achieved. Results obtained with two different masks are shown in Fig. 7.

In another demonstration we determined the shape of the wavefront of a collimated beam reflected from a concave

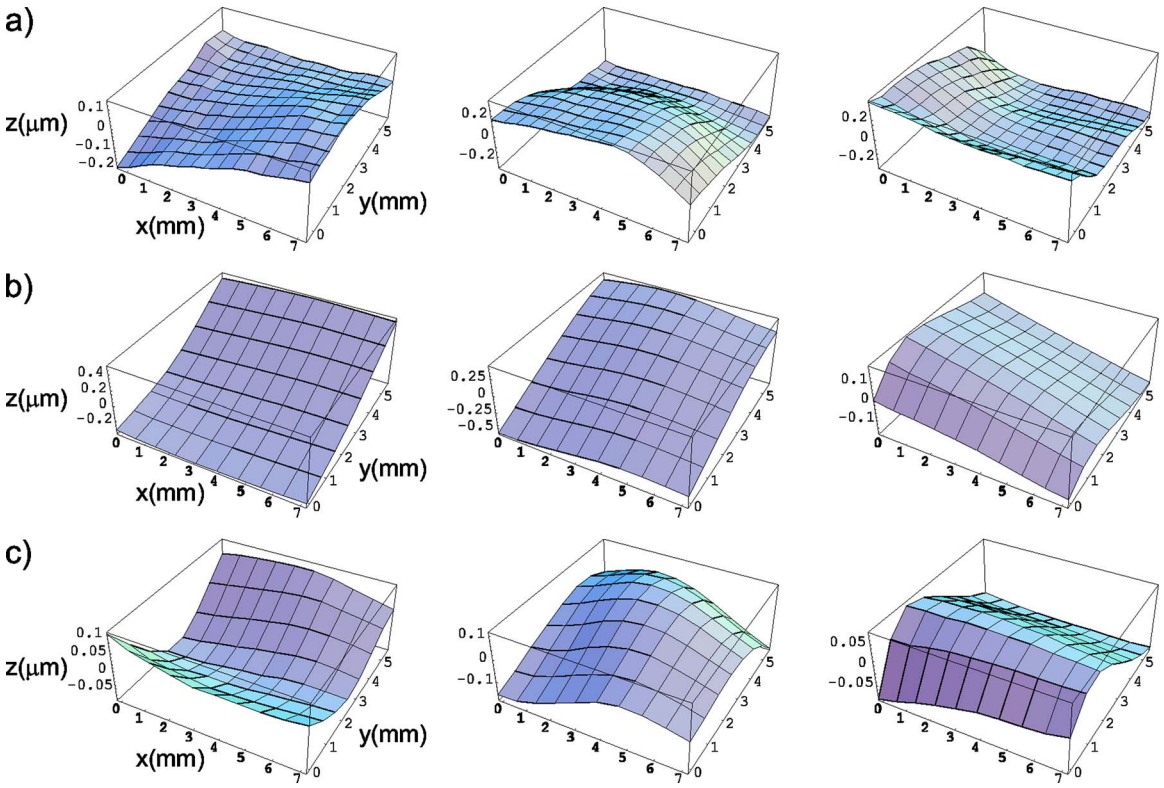

Fig. 7. Sample distortions of the wavefront of a collimated laser beam propagating in a turbulent air flow induced by a soldering iron located beneath the beam. The focal lengths of the zone plates used are equal to (a) 10 cm and (b) 13 cm. (c) The wavefronts shown in (b) after subtracting a flat, tilted wavefront.

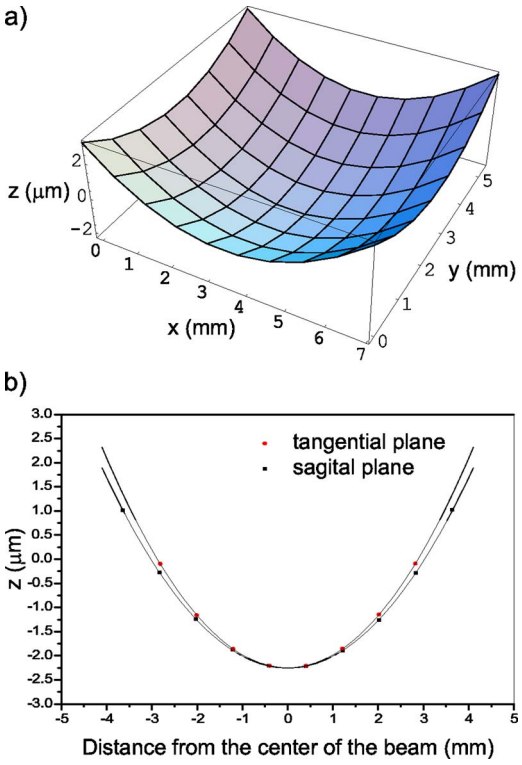

Fig. 8. (a) The wavefront of a collimated beam reflected from a spherical mirror with an angle of incidence of 14.7°. (b) The sections of the wavefront in the tangential and sagittal planes.

spherical mirror of focal length $f=250$ cm. For the angle of incidence $\theta \neq 0$ the mirror introduces astigmatism and two different foci, tangential and sagittal, appear. Their distance from the mirror is approximately equal to the corresponding focal lengths:

$$f_t = f \cos \theta \tag{6a}$$

$$f_s = f/\cos \theta. \tag{6b}$$

The angle of incidence was equal to 14.7°. Therefore the tangential and sagittal foci were approximately 242 and 258 cm away from the mirror, respectively. The Shack–Hartmann sensor mask was located 47 cm away from the mirror. Thus the expected curvature radii were ≈195 and ≈211 cm. The reference image of the spots was recorded with the concave mirror replaced by a flat one. The reconstructed wavefront is shown in Fig. 8(a) and sections of the wavefront in the tangential and sagittal planes together with the fitted function describing a circular arc are shown in Fig. 8(b). The curvature radii resulting from the fit are slightly shorter than expected and are equal to 184 and 203 cm, respectively. The 5% error probably originates from the fact that the wavefront of the incident beam was not absolutely flat at the mirror, although it was collimated as well as possible within the size of the laboratory room. However, the main goal of this experiment, the demonstration of the astigmatism introduced by a spherical mirror set at an angle to the beam, was easily accomplished.

If the setup is built on an optical bench instead of a table, the use of a mirror could be difficult. A lens with a long enough focal length can be inserted into the beam and tilted by a proper angle to obtain the same result.

VII. CONCLUSIONS

We have proposed a simple and low cost method of building an optical wavefront sensor based on a Shack–Hartman detector in which the array of lenslets is replaced by a mask consisting of Fresnel zone plates. The mask can be easily prepared by students during a laboratory course using either a photographic or polygraphic technique.

In spite of its simplicity the technique achieves a sensitivity of $\lambda/50$ in relative measurements, which is sufficient to demonstrate the distortions of the wavefront caused by fluctuations of the air density and temperature during turbulent flow. Also, the effect of optical components on the shape of the wavefront can be easily characterized qualitatively and quantitatively.

We suggest that an experiment involving mask making and its use to measure different wavefronts be included in an undergraduate laboratory. This use would deepen students' understanding of the concept of a wavefront and make them familiar with techniques widely used in adaptive optics, eye surgery, and high energy lasers. One possible extension of this experiment involves a deformable mirror and a feedback loop to illustrate the principles of adaptive optics.

ACKNOWLEDGMENT

This work was supported by the Polish Ministry of Science and Higher Education, Grant No. N202 019 32/0698.

[a]Electronic mail: fita@fuw.edu.pl

[1] W. Tomlinson, "Applications of GRIN-rod lenses in optical fiber communication systems," Appl. Opt. **19**, 1127–1139 (1980).
[2] F. Roddier, *Adaptive Optics in Astronomy* (Cambridge University Press, Cambridge, 1999).
[3] F. Druon, G. Cheriaux, J. Faure, J. Nees, M. Nantel, A. Maksimchuk, G. Mourou, J. Chanteloup, and G. Vdovin, "Wave-front correction of femtosecond terawatt lasers by deformable mirrors," Opt. Lett. **23**, 1043–1045 (1998).
[4] H. Baumhacker, G. Pretzler, K. Witte, M. Hegelich, M. Kaluza, S. Karsch, A. Kudryashov, V. Samarkin, and A. Roukossouev, "Correction of strong phase and amplitude modulations by two deformable mirrors in a multistaged Ti:sapphire laser," Opt. Lett. **27**, 1570–1572 (2002).
[5] J. Liang, B. Grimm, S. Goelz, and J. F. Bille, "Objective measurement of wave aberrations of the human eye with the use of a Hartmann-Shack wave-front sensor," J. Opt. Soc. Am. A **11**, 1949–1957 (1994).
[6] J. Schwiegerling and D. R. Neal, "Historical development of the Shack-Hartmann wavefront sensor," in *Robert Shannon and Roland Shack: Legends in Applied Optics*, edited by J. E. Harvey and R. B. Hooker (SPIE, Bellingham, WA, 2005), pp. 132–139.
[7] B. C. Platt and R. S. Shack, "History and principles of Shack-Hartmann wavefront sensing," J. Refract. Surg. **17**, 573–577 (2001).
[8] D. R. Neal, "Shack-Hartmann sensor engineered for commercial measurement applications," in *Robert Shannon and Roland Shack: Legends in Applied Optics*, edited by J. E. Harvey and R. B. Hooker (SPIE, Bellingham, WA, 2005), pp. 139–160.
[9] O. E. Myers, "Studies of transmission zone plates," Am. J. Phys. **19**, 359–365 (1951).
[10] M. Sussman, "Elementary diffraction theory of zone plates," Am. J. Phys. **28**, 394–398 (1960).
[11] H. M. Childers and D. E. Stone, "Solution to the Fresnel zone plate problem," Am. J. Phys. **37**, 721–726 (1969).
[12] J. Higbie, "Fresnel zone plate: Anomalous foci," Am. J. Phys. **44**, 929–930 (1976).
[13] C. W. Clark and Y. N. Demkov, "Making zone plates with a laser printer," Am. J. Phys. **59**, 158–162 (1991).
[14] K. D. Mielenz, "Algorithms for Fresnel diffraction at rectangular and circular apertures," J. Res. Natl. Inst. Stand. Technol. **103**, 497–509 (1998).

[15] D. M. Topa, "Optimized methods for focal spot location using center-of-mass algorithms," Proc. SPIE **4769**, 116–129 (2002). Also available at ⟨www.wavefrontsciences.com/papers.htm⟩.
[16] Glenn A. Tyler, "Reconstruction and assessment of the least-squares and slope discrepancy components of the phase," J. Opt. Soc. Am. A **17**, 1828–1839 (2000).
[17] J. Herrmann, "Least-squares wave front errors of minimum norm," J. Opt. Soc. Am. **70**, 28–35 (1980).
[18] W. H. Southwell, "Wave-front estimation from wave-front slope measurements," J. Opt. Soc. Am. **70**, 998–1006 (1980).

ONLINE COLOR FIGURES AND AUXILIARY MATERIAL

AJP uses author-provided color figures for its online version (figures will still be black and white in the print version). Figure captions and references to the figures in the text must be appropriate for both color and black and white versions. There is no extra cost for online color figures.

In addition AJP utilizes the Electronic Physics Auxiliary Publication Service (EPAPS) maintained by the American Institute of Physics (AIP). This low-cost electronic depository contains material supplemental to papers published through AIP. Appropriate materials include digital multimedia (such as audio, movie, computer animations, 3D figures), computer program listings, additional figures, and large tables of data.

More information on both these options can be found at www.kzoo.edu/ajp/.